RESEARCH ARTICLE

VOLCANICA

The thermal properties of submarine rhyolite lavas from Havre volcano (Kermadec arc, Pacific Ocean)

Rebecca J. Carey*[α], Michael J. Heap†[β,γ], Samuel J. Mitchell[δ], and Fabian B. Wadsworth[ε]

[α]School of Natural Sciences and CODES, University of Tasmania, Hobart, Tasmania 7001, Australia.
[β]Université de Strasbourg, CNRS, Institut Terre et Environnement de Strasbourg, UMR 7063, 5 rue Descartes, Strasbourg F-67084, France.
[γ]Institut Universitaire de France (IUF), Paris, France.
[δ]School of Earth Sciences, Wills Memorial Building, University of Bristol, Bristol BS8 1RJ, UK.
[ε]Earth & Environmental Sciences, Ludwig-Maximilians-Universität München, Theresienstr. 41, 80333 Munich, Germany.

Abstract

The thermal properties of lavas are required for modelling volcanic and hydrothermal processes, yet are scarce for submarine lavas. Laboratory experiments, using the transient hot-strip method, are used to understand the role of porosity, glass content, and pore fluid type on the thermal properties of submarine lavas from Havre volcano. Thermal diffusivity and specific heat capacity do not change systematically with porosity; however, thermal conductivity decreases as porosity increases. The thermal conductivity of the submarine lavas is lower than for subaerial lavas with the same porosity, a consequence of their higher glass contents. We show that, using our data and effective medium models, the thermal properties of any lava can be estimated as long as their porosity, glass content, and void-filling fluid phase is known. This approach can be used to estimate properties for multiphase models for submarine eruption dynamics, hydrothermal system hydrology, cooling timescales, and heat flux calculations.

Keywords: Rhyolite lava; Thermal conductivity; Thermal diffusivity; Specific heat capacity.

Submitted: 2024-07-10 | Accepted: 2025-03-07 | Published: 2025-06-27

Editor: A. Graettinger | Typesetter: J. Farquharson

1 Introduction

The thermal properties of volcanic rocks are an important input parameter in a wide range of models designed to understand heat transfer in active volcanoes [Irvine 1970; Norton and Knight 1977; Huppert and Sparks 1981; Carrigan 1984; Bruce and Huppert 1989; Carrigan et al. 1992; Wooster et al. 1997; Fialko and Rubin 1999; Annen et al. 2008; Nabelek et al. 2012; Annen 2017; Tsang et al. 2019; Loncar and Huppert 2022] and geothermal reservoirs [Canet et al. 2015; Gunnarsson and Aradóttir 2015; Carlino et al. 2016; Vélez et al. 2018; Burchardt et al. 2022; González et al. 2022]. The accuracy of these models depends, in part, on the assumed values for the thermal properties of the rocks in question and, very often, these values are provided by experimental studies. Indeed, a number of experimental studies have sought to better understand the thermal properties of volcanic rocks [Horai et al. 1970; Fujii and Osako 1973; Robertson and Peck 1974; Bagdassarov and Dingwell 1994; Whittington et al. 2009; Romine et al. 2012; Lenhardt and Götz 2015; Mielke et al. 2015; Hofmeister et al. 2016; Mielke et al. 2016; Balkan et al. 2017; Mielke et al. 2017; Vélez et al. 2018; Heap et al. 2020; Weydt et al. 2021; Heap et al. 2022; Weydt et al. 2022; Heap et al. 2023]. These studies for volcanic rocks from subaerial volcanoes have, for example, shown that thermal conductivity and thermal diffusivity are lower at high porosity compared with low porosity [e.g. Robertson and Peck 1974; Heap et al. 2020], and that this porosity control on thermal properties appears to be first-order and dominates over changes in, for example, the hydrothermal alteration of lavas [Heap et al. 2022]. In the terrestrial realm, the thermal properties of volcanic rocks—and its dependence on porosity—is typically sufficient to model heat flow (see references above). Given that the porosity of submarine lavas and clasts are not substantially different from subaerial lavas [e.g. Yokose et al. 2005; White et al. 2015], their thermal properties may be similar; but this has not yet been tested experimentally. The thermal properties of submarine lavas will provide more reliable multiphase model outputs for cooling dynamics of submarine lavas and subsequent flow morphologies [e.g. Griffiths and Fink 1992], and larger Earth system processes such as submarine eruption dynamics, hydrothermal system hydrology, and heat flux from the mid-ocean ridge system.

Here, therefore, we provide new thermal property data (thermal conductivity, thermal diffusivity, and specific heat capacity) for rhyolite lavas collected from a deep submarine volcano: Havre volcano (Tonga-Kermadec Arc, Pacific Ocean). We aim to use effective medium models to both encapsulate these new data in constitutive laws for thermal properties, and also to compare these new data with those for subaerial volcanoes. We use our data to discuss lava crust development and the cooling of lava domes, and provide recommendations for those tasked with modelling heat transport in submarine volcanic systems.

2 Havre volcano (Kermadec arc Pacific Ocean)

The Havre submarine volcano is situated within the Kermadec volcanic arc, which extends to the north of New Zealand (Figure 1). This volcano rises from a ~2500 m seafloor and has a 5 km-wide caldera characterised by rim and floor depths of approximately 1000 and 1500 metres below sea level (m.b.s.l.), respectively [Wright et al. 2006]. Havre volcano has only ex-

*rebecca.carey@utas.edu.au
†heap@unistra.fr

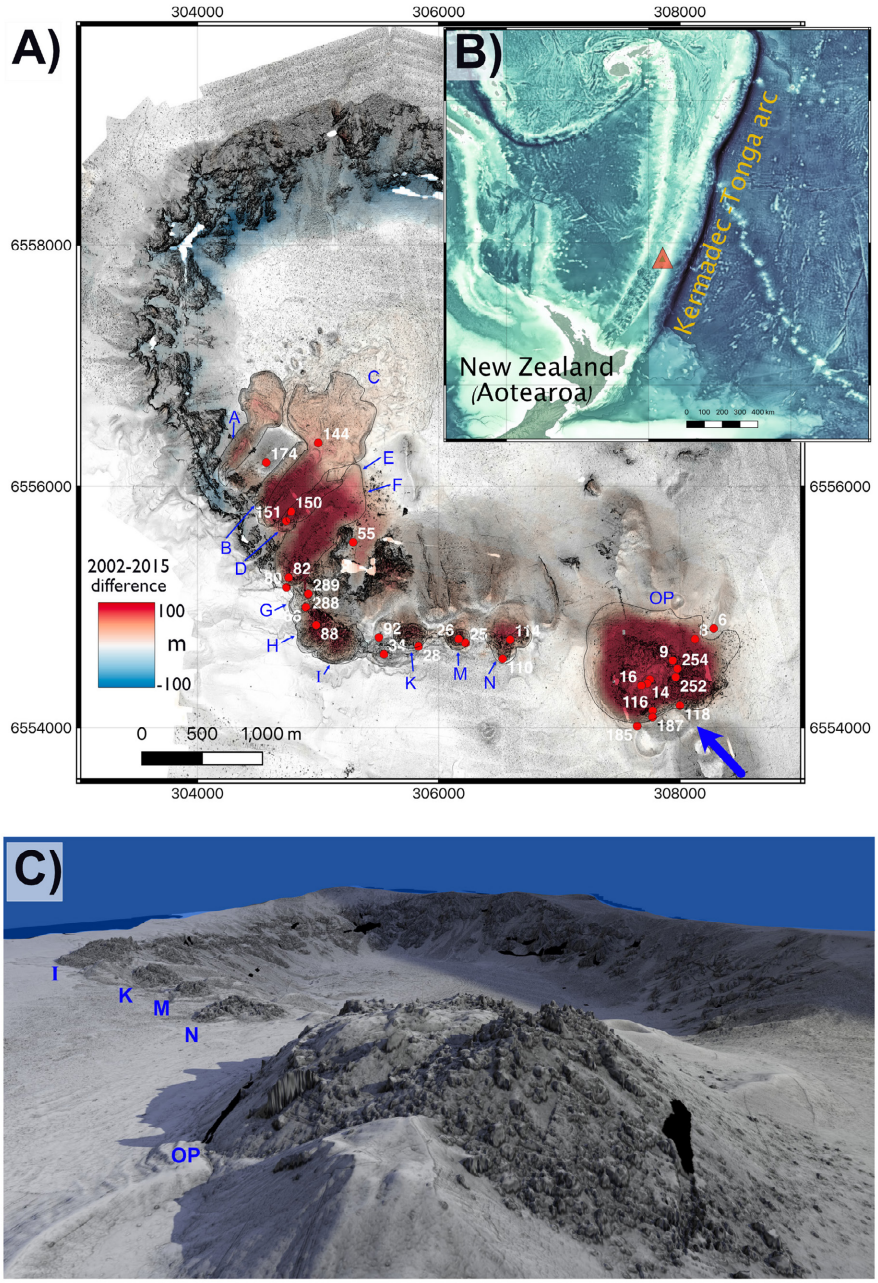

Figure 1: [A] Bathymetric difference map of Havre volcano using pre- and post 2012 eruption bathymetry datasets. Eruption products are indicated by the height difference colours and outlines. Lavas A-OP are highlighted in blue. Locations of samples shown as red circles. [B] Location of Havre volcano (red triangle) in the Kermadec Arc. [C] 3D rendered topographical image with view towards the NW (blue arrow). The Dome OP is 250 m-high and 1 km-wide. The caldera floor in the background lies at 1519 m below sea level.

perienced one known eruption, which occurred in 2012 [GVP 2012; Carey et al. 2014]. This eruption was detected through the presence of a vast 400 km^2 pumice raft composed of rhyolite pumice that dispersed across the Pacific Ocean [GVP 2012; Jutzeler et al. 2014; Manga et al. 2018a].

Four surveys of the Havre submarine volcano have been conducted. These surveys took place in 2002, 2012, 2015, and 2022 [Wright et al. 2006; Carey et al. 2014; 2018]. The 2015 survey utilised both remote and autonomous vehicles to investigate the caldera geomorphology and the geometry of the 2012 eruption products, and to collect samples from stratigraphic units from the caldera wall and the 2012 eruption products.

The comparison between multibeam bathymetry data collected in 2002 by ship-based sensors and the post-eruption 1 m-scale resolution bathymetry data acquired through the Autonomous Underwater Vehicle (AUV) Sentry has illustrated the distribution of the 2012 eruption products on the seafloor

[Carey et al. 2018; Spain et al. 2025]. This high-resolution AUV Sentry data, combined with visual observations and collected lava samples has demonstrated that a total of 15 separate lavas and domes resulted from the 2012 eruption, originating from 14 distinct vents situated at depths ranging from 880 to 1280 m.b.s.l [Ikegami et al. 2018]. Thirteen (13) of these lavas were found to be concentrated along the caldera ring fault segments, primarily on the south and southwest sides of the caldera.

Two distinct morphologies were identified among these lavas. Lavas that flowed down ~15–30-degree steep caldera walls at an approximate angle of 15 degrees, resulted in the formation of long lobate lavas, while others erupted on relatively flat surfaces, are either short lobate lavas or domes. One dome, "Dome OP", a large coalesced dome measuring 1 km in width and 250 m in height, features two observable lobes (O and P). All domes and lavas have both coherent and autobreccia facies (Figure 2). Dome OP was observed to have a substantial circular apron of talus, presumably deposited during its growth. Ikegami et al. [2018] demonstrated that there were no morphological differences between Havre submarine lavas and domes with subaerial analogues emplaced on the same slope angles.

Remotely Operated underwater Vehicle (ROV) and AUV mapping and sample observations also found altered pre-2012 lavas on the southern caldera rim [Ikegami et al. 2018]. The caldera walls at depths between 1515 and 900 m.b.s.l are dominantly composed of coherent volcanic and intrusive rocks of unknown composition, together with minor widespread planar and cross bedded felsic units. The eruption history of these products is currently being investigated.

3 Materials and Methods

The samples in this study were collected in 2015 within and on the Havre submarine caldera using ROV Jason (WHOI). The samples were collected from in-situ domes and lavas, autobreccia adjacent to coherent lava facies, or talus from around the domes and lavas (Figure 1 and 2). In this manuscript, we use the term "lava" to describe the cooled rocks from a lava flow or lava dome. Samples were collected via ROV manipulators and have an average diameter of 10–30 cm. Thirty (30) samples were cut for the thermal property analysis presented here. Three samples are from pre-2012 domes and caldera wall stratigraphy, with the remaining 27 from the 2012 lavas.

All of the 2012 products are rhyolitic in composition (70–72 wt.% SiO_2) [Carey et al. 2018]. Scanning electron microscope (SEM) images of the 2012 lavas illustrate highly variable microtextures which is consistent with the diversity of the sample collection (Figure 3). The samples are light grey to very dark grey in colour and have between 5 and 7 % phenocrysts of quartz, feldspar, rare pyroxene, and Fe-Ti oxides [Ikegami et al. 2018]. All rocks have euhedral to needle-shaped plagioclase microlites with abundances between just a few area% (HVR085) and a completely microcrystalline groundmass (HVR055). The total bulk porosities of the samples range from 0.11 to 0.43 (Table 1). Most of the samples feature secondary vapour-phase cristobalite within the large vesicles [Manga et al. 2018b], which can be observed to sometimes occlude the void space. The microtextures of the samples also show variable amounts of cristobalite present in diktytaxitic voids between microlites. The cristobalite varies in size between 10 and 100 µm in diameter. Fractures in the hand samples and groundmass are present in some samples. The samples collected from pre-2012 domes (HVR092, HVR080) and the caldera wall (HVR174) are variably hydrothermally altered. HVR080 is grey-yellow in colour, contains clay and zeolites, is devoid of cristobalite and glass, and the phenocrysts, microphenocrysts, and microlites are cemented with clay. HVR174 and HVR092 are grey with some outer discoloration and have microtextures that include glass, with <10 area% microlites and microphenocrysts, but lack cristobalite.

A photograph of each block in-situ (taken by the ROV during sample collection), a photograph of each block, and additional backscattered scanning electron microscope images for each block are available in the Supplementary Information.

Two cylindrical samples (20 mm in diameter and 20–40 mm in length) were prepared from 26 of the 30 blocks collected. For the remaining four blocks, only one cylindrical sample could be prepared. These samples were washed and then dried in a vacuum-oven at 40 °C for at least 48 h. Once dry, the dry mass and dimensions (length and radius) of each sample was measured using a balance and digital callipers, respectively. The dry bulk density of the samples, ρ_b, was then calculated using the dry mass and bulk sample volume assuming perfect cylinder geometry. Finally, the connected porosity of each sample was calculated using the bulk sample volume and the connected skeletal (solid) sample volume measured by a helium pycnometer (an AccuPyc II from Micromeritics®). Offcuts from each block were powdered using a Mixer Mill 400 from Retsch® and volumes of aliquots of known mass were measured using the helium pycnometer to provide the solid density of each block. The bulk density of each sample and the solid density of the parent block were then used to determine the total porosity of each sample. Isolated porosity was determined by subtracting the connected porosity from the total porosity.

The thermal conductivity λ (in units of $W\,m^{-1}\,K^{-1}$) and thermal diffusivity D (in units of $mm^2\,s^{-1}$) of the samples were measured using a Hot Disk® TPS 500 Thermal Constants Analyser using the transient plane source (TPS) method [Gustafsson 1991; Harlé et al. 2019; Heap et al. 2020; 2022]. The TPS method, a periodic method of thermal property measurement, uses a resistive sensor (the transient plane source) sandwiched between two samples to measure the increase in resistance as it heats the samples using an electrical current pulse. Because the geometry of the sensor is known, the average temperature increase as a function of time can be calculated, which can be then used to determine the thermal conductivity. The resistive sensor is therefore used as both the heat source and the temperature sensor. In our setup, the resistive sensor consists of two 10 µm-thick nickel foil spirals (radius of 3.189 mm) that are encased and insulated by 30 µm-thick Kapton (see inset in Figure 4). Measurements were made by sandwiching the sensor between two cylindrical samples cored from the same block (Figure 4); for the four blocks from which only one cylindrical sample could be pre-

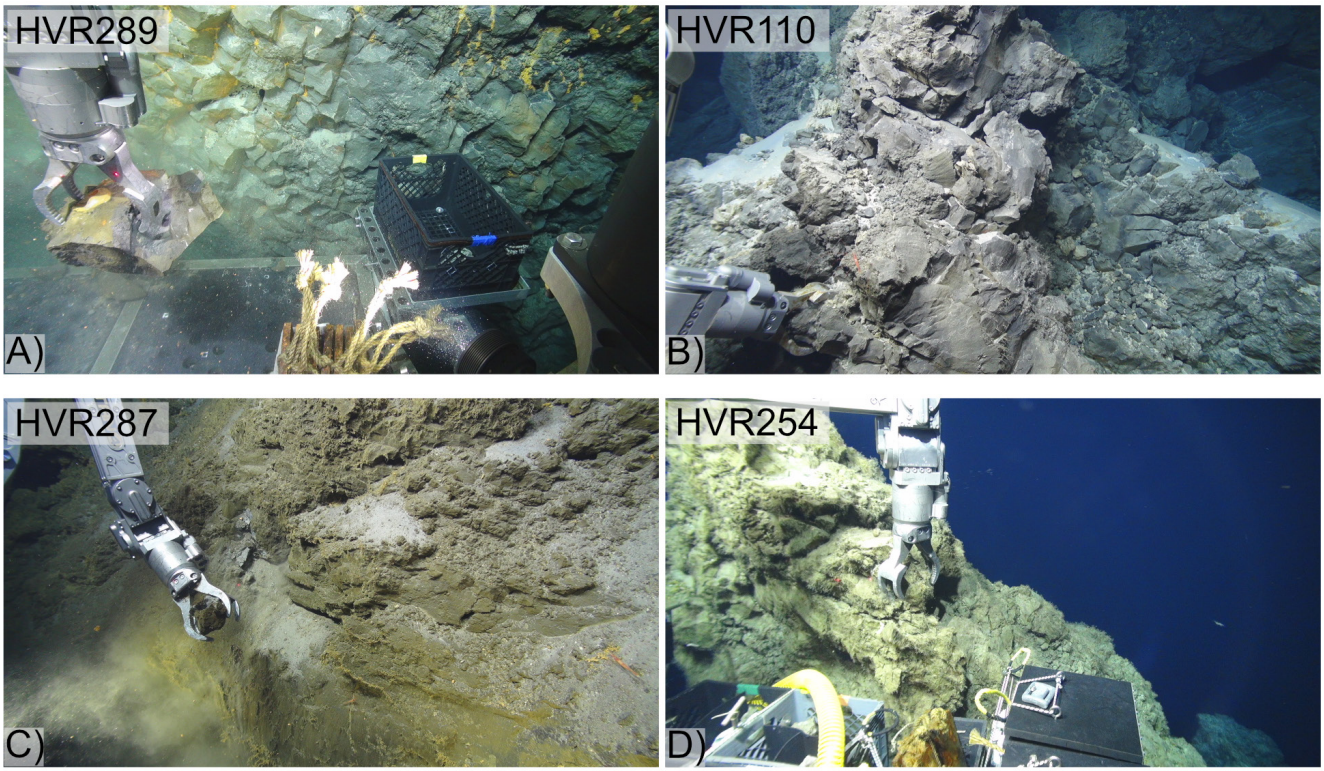

Figure 2: High-definition images taken during sample collection at Havre volcano using the camera on the Remotely Operated underwater Vehicle (ROV). Samples were taken by ROV manipulator from all 2012 and pre-2012 in-situ lavas encountered during 13 dives on the volcano. ROV Claw diameter = 15 cm.

pared, we sandwiched the sensor between the solitary sample and an offcut from the parent block. A good contact between the sensor and the surface of the samples was ensured by tightening a screw positioned at the top of the sample jig. An electrical current of known power and for a fixed duration was then passed through the sensor, which recorded the increase in sample temperature as a function of time. The output power and test duration used were 80–220 mW and 5–10 s, respectively. Four consecutive measurements were performed on each sample pair (on the four different combinations of sample end-faces), and we report herein the mean and standard deviation from the mean of these four measurements. Each measurement was performed at least 10–15 minutes apart to ensure that the samples and sample assembly had re-equilibrated to the target temperature. The specific heat capacity, C_p (in units of $\mathrm{J\,kg^{-1}\,K^{-1}}$), was calculated using $C_p = k/(\rho_b D)$. We used the Isotropic Hot Disk® Measurement Module for all measurements.

The standard uncertainty for values of thermal conductivity and thermal diffusivity using the transient hot-strip method has been determined to be 2.6 and 11 %, respectively [Hammerschmidt and Sabuga 2000]. Measurement uncertainty using this technique arises from contact losses and ballistic radiative transfer gains [Hofmeister 2018]. The standard error for the thermal conductivity measured using our Hot Disk® TPS 500 Thermal Constants Analyser, assessed by measuring the same reference sandstone sample 100 times, was estimated to be 0.007 $\mathrm{W\,m^{-1}\,K^{-1}}$ [Heap et al. 2023].

4 Results

In this section, we present the porosity results followed by the measurements of thermal conductivity, thermal diffusivity, and specific heat capacity as a function of total porosity.

The connected and total porosities of the lavas from Havre volcano vary from 0.03 to 0.44 and from 0.11 to 0.45, respectively (Figure 5). A large proportion of the lavas contain isolated porosity, which varies in these samples from 0 to 0.09 (Figure 5). Although the amount of isolated porosity does not vary systematically as a function of connected porosity (Figure 5), we note that, for the low-porosity samples, the isolated porosity represents a larger proportion of the total porosity than for the high-porosity samples.

Thermal conductivity, thermal diffusivity, and specific heat capacity are plotted as a function of total porosity in Figure 6A–6C, respectively (data available in Table 1). The data are split between those samples collected from, or near, dome OP (black diamonds on Figure 6) and those collected from elsewhere on the volcano (white and yellow diamonds on Figure 6) (see Figure 1 for a map of the collection sites). We make this demarcation simply because the bulk of the samples are from dome OP. We find that thermal conductivity decreases from ~1.1 to ~0.5 $\mathrm{W\,m^{-1}\,K^{-1}}$ as total porosity is increased from ~0.1 to ~0.45 (Figure 6A). Thermal diffusivity remains more-or-less constant as total porosity is increased from ~0.1 to ~0.45. Specific heat capacity remains between 0.65 and 0.9 $\mathrm{J\,kg^{-1}\,K^{-1}}$ for all samples, and does not appear to change sys-

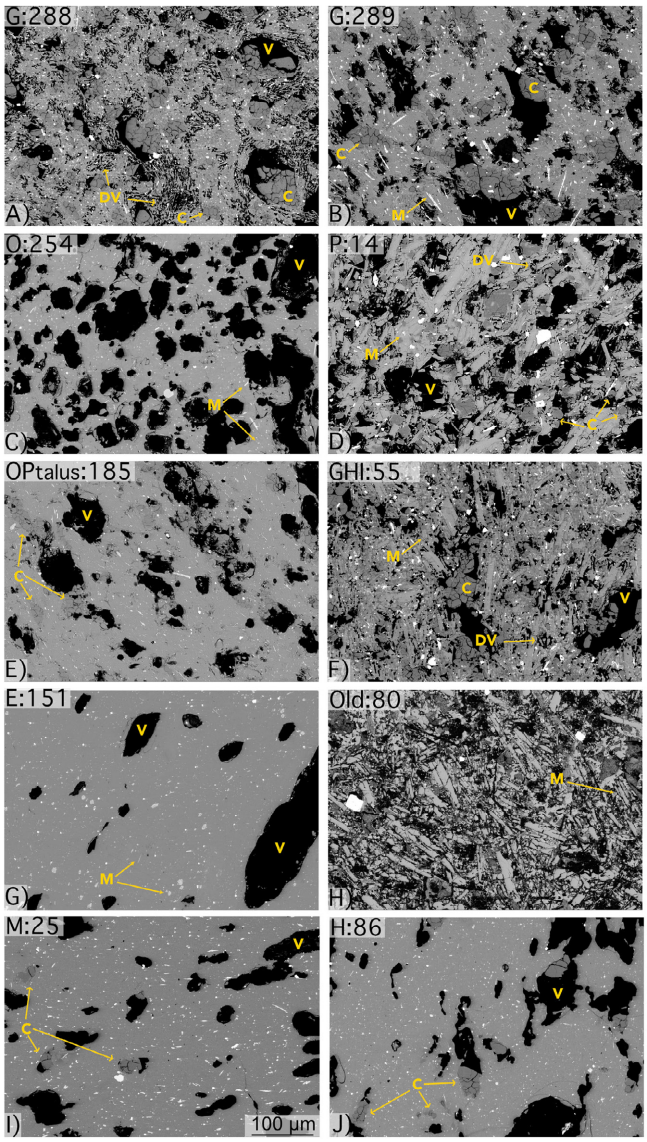

Figure 3: Suite of backscattered scanning electron microscope images illustrating the diversity of textures, isolated and total porosity, cristobalite, and microlite contents. Letters relate to lava nomenclature (A-P), with sample numbers. Old = pre-2012 lava and is clay rich with no glass remaining. Sampling locations shown in Figure 1. C=cristobalite, DV = diktytaxitic voids, V = vesicle, M = microlite. Note how the cristobalite occludes the pore space or replaces groundmass glass. Zones of diktytaxitic voids surround or are immediately adjacent to vesicles.

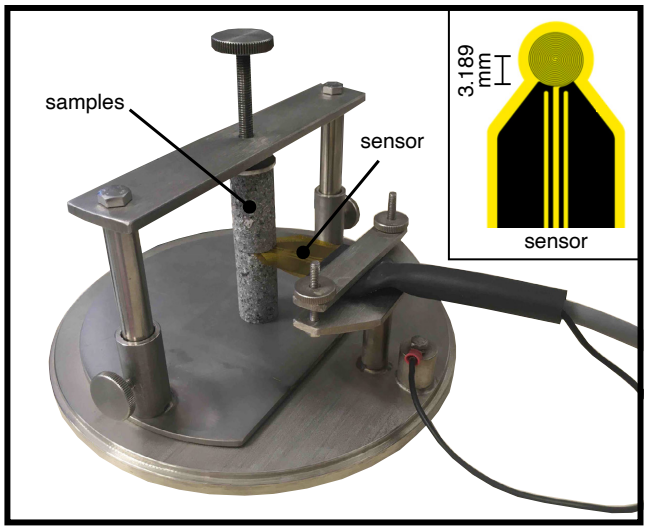

Figure 4: Photograph of the experimental setup for the measurements. Inset in the top right-hand corner shows a zoomed-in image of the sensor used, consisting of two 10 µm-thick nickel foil spirals (radius of 3.189 mm) that are encased and insulated by 30 µm-thick kapton. The screw on the top of the setup ensures a good contact between the sensor and the samples.

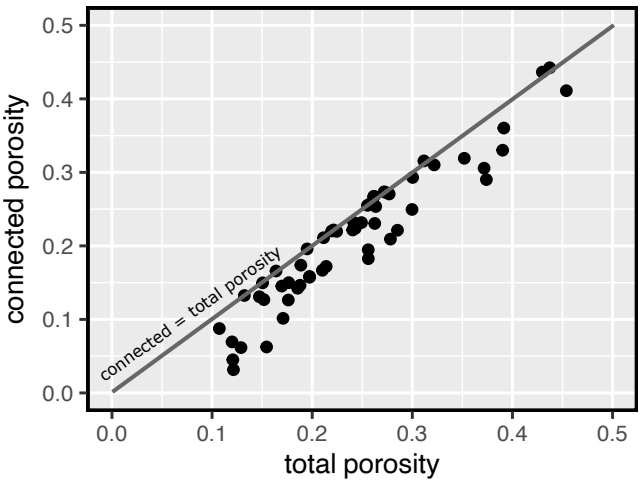

Figure 5: Total porosity as a function of connected porosity for the suite of lavas from Havre volcano.

tematically as a function of porosity (Figure 6C). Finally, we note that there is essentially no difference (i.e. the data are not clustered) between the thermal properties of the samples collected from dome OP and those collected elsewhere on the volcano (Figure 5).

5 Discussion

5.1 Comparisons between the thermal properties of submarine and subaerial volcanoes

Our new data show that the thermal conductivity of lavas from Havre volcano decreases, and that the thermal diffusivity and specific heat capacity remain more-or-less constant, as a function of total porosity (Figure 5). Previous studies of lavas from subaerial volcanoes have also shown that the thermal conductivity [e.g. Robertson and Peck 1974; Heap et al. 2020; 2022] decreases as porosity is increased up to 0.95, and that both the thermal diffusivity and specific heat capacity are largely unchanged up to a porosity of ~0.6 [e.g. Heap et al. 2020; 2022]. Previous studies have also shown that hydrothermal alteration can reduce the thermal conductivity of volcanic rocks [e.g. Heap et al. 2022; 2023]. The lavas from Havre volcano measured for this study contain variable quantities of cristobalite (Figure 3), and one of the older lavas from the crater wall (HVR080) is very hydrothermally altered. Regardless of

Table 1: Thermal conductivity, thermal diffusivity, and specific heat capacity for the lavas collected from Havre volcano (see map in Figure 1 for sampling locations). Also provided are connected and total porosity of each of the two cylindrical samples used for the measurement. For measurements that used one cylindrical sample and an offcut from the parent block, only the connected and total porosity of the cylindrical sample is shown (the porosity of the offcut was not determined). The average connected and total porosities of the two samples are also provided (when only one cylindrical sample was used, the average porosities are simply equal to the porosity of this sample). The thermal conductivity of each sample pair (or sample and offcut) was measured four times and we report the mean and standard deviation of the mean for these four measurements. Measurements were collected under ambient pressure and temperature conditions. Data are available in the Microsoft Excel spreadsheet that accompanies this contribution as Supplementary Material 1.

Sample name	Locality	Porosity						Thermal conductivity ($W m^{-1} K^{-1}$)	Thermal diffusivity ($mm^2 s^{-1}$)	Specific heat capacity ($J kg^{-1} K^{-1}$)
		Connected			Total					
		Sample 1	Sample 2	Average	Sample 1	Sample 2	Average			
HVR144	C	0.06	0.03	0.05	0.15	0.12	0.14	1.04 ± 0.003	0.60 ± 0.042	0.83 ± 0.061
HVR150	D	0.09	-	0.09	0.11	-	0.11	1.01 ± 0.014	0.61 ± 0.033	0.74 ± 0.050
HVR151	E	0.07	0.17	0.12	0.12	0.21	0.17	0.93 ± 0.122	0.53 ± 0.062	0.86 ± 0.135
HVR082	F	0.13	0.10	0.11	0.18	0.17	0.17	0.85 ± 0.070	0.58 ± 0.152	0.74 ± 0.144
HVR288	G	0.27	0.27	0.27	0.26	0.26	0.26	0.88 ± 0.013	0.59 ± 0.023	0.78 ± 0.021
HVR289	G	0.22	0.22	0.22	0.22	0.22	0.22	0.94 ± 0.060	0.60 ± 0.067	0.78 ± 0.039
HVR086	H	0.22	0.22	0.22	0.24	0.24	0.24	0.82 ± 0.124	0.54 ± 0.014	0.80 ± 0.120
HVR088	H	0.23	0.23	0.23	0.25	0.24	0.25	0.79 ± 0.080	0.57 ± 0.034	0.74 ± 0.058
HVR034	I	0.17	0.16	0.16	0.21	0.20	0.20	0.83 ± 0.049	0.57 ± 0.012	0.72 ± 0.055
HVR092	older (J)	0.15	0.16	0.15	0.19	0.20	0.19	0.83 ± 0.128	0.53 ± 0.079	0.78 ± 0.070
HVR055	HIJ megablock	0.26	0.26	0.26	0.26	0.26	0.26	0.98 ± 0.062	0.64 ± 0.032	0.80 ± 0.014
HVR028	K	0.31	0.29	0.30	0.32	0.30	0.31	0.62 ± 0.066	0.52 ± 0.031	0.72 ± 0.090
HVR025	M	0.14	0.23	0.19	0.19	0.26	0.22	0.87 ± 0.018	0.52 ± 0.022	0.87 ± 0.047
HVR026	M	0.15	-	0.15	0.18	-	0.18	0.89 ± 0.110	0.64 ± 0.089	0.70 ± 0.182
HVR110	N	0.06	0.05	0.05	0.13	0.12	0.12	1.07 ± 0.015	0.65 ± 0.015	0.77 ± 0.029
HVR114	N	0.13	0.15	0.14	0.15	0.17	0.16	0.96 ± 0.057	0.70 ± 0.069	0.66 ± 0.079
HVR016	O	0.13	0.15	0.14	0.13	0.15	0.14	1.08 ± 0.048	0.59 ± 0.009	0.83 ± 0.029
HVR254	O	0.33	0.31	0.32	0.39	0.37	0.38	0.55 ± 0.030	0.56 ± 0.070	0.66 ± 0.126
HVR009	OP	0.32	-	0.32	0.31	-	0.31	0.86 ± 0.005	0.59 ± 0.018	0.82 ± 0.030
HVR013	OP	0.27	0.27	0.27	0.27	0.27	0.27	0.92 ± 0.071	0.65 ± 0.019	0.74 ± 0.036
HVR116	OP	0.20	0.17	0.18	0.19	0.16	0.18	0.95 ± 0.082	0.63 ± 0.027	0.73 ± 0.035
HVR118	OP	0.32	0.25	0.28	0.35	0.30	0.33	0.65 ± 0.079	0.50 ± 0.052	0.81 ± 0.045
HVR252	OP	0.19	0.21	0.20	0.26	0.28	0.27	0.75 ± 0.026	0.54 ± 0.015	0.78 ± 0.034
HVR006	OP Talus	0.25	0.27	0.26	0.26	0.28	0.27	0.78 ± 0.086	0.57 ± 0.043	0.76 ± 0.056
HVR008	OP Talus	0.29	-	0.29	0.37	-	0.37	0.60 ± 0.015	0.53 ± 0.019	0.76 ± 0.046
HVR185	OP Talus	0.13	0.17	0.15	0.15	0.19	0.17	0.94 ± 0.030	0.61 ± 0.047	0.74 ± 0.041
HVR187	OP Talus	0.41	0.36	0.39	0.45	0.39	0.42	0.53 ± 0.148	0.60 ± 0.130	0.67 ± 0.289
HVR014	P	0.21	0.22	0.22	0.21	0.22	0.22	1.06 ± 0.041	0.65 ± 0.009	0.80 ± 0.026
HVR080	older	0.44	0.44	0.44	0.43	0.44	0.43	0.57 ± 0.009	0.49 ± 0.039	0.76 ± 0.063
HVR174	older	0.22	0.18	0.20	0.29	0.26	0.27	0.86 ± 0.012	0.55 ± 0.044	0.81 ± 0.066

the degree of hydrothermal alteration, we find that all samples lie on the same trend as a function of porosity, including sample HVR080 (the yellow diamond on Figure 6; Table 1).

We compare our new thermal property data for lavas from Havre volcano with those published for subaerial volcanoes in Figure 7. The data for subaerial volcanoes include altered andesites from La Soufrière de Guadeloupe (Eastern Caribbean [Heap et al. 2022]), andesites from Mt Ruapehu (New Zealand [Heap et al. 2020]), altered basaltic-andesites from Mt Merapi (Indonesia [Heap et al. 2020]), dacites from Chaos Crags (USA [Heap et al. 2022]), and basalts from several volcanoes in Hawai'i (USA [Robertson and Peck 1974]). The thermal conductivity data shown in Figure 7A show that the thermal conductivities of the lavas from Havre volcano are similar to those measured for the suite of subaerial volcanoes, although, for a given porosity, the lavas from Havre volcano are typically lower than those for the subaerial volcanoes. The thermal diffusivity (Figure 7B) and specific heat capacity (Figure 7C) of the lavas from Havre volcano are very similar to those measured for subaerial volcanoes.

To better understand the relationship between the thermal properties and the porosity for the lavas from Havre volcano, we can use an effective medium approach that has been successfully used to describe the thermal properties of volcanic rocks from subaerial volcanoes [Heap et al. 2020; 2022]. If these effective medium approaches can also well describe the lavas from Havre volcano, then we could conclude the relationship between thermal properties and porosity is similar for volcanic rocks from submarine and subaerial volcanoes.

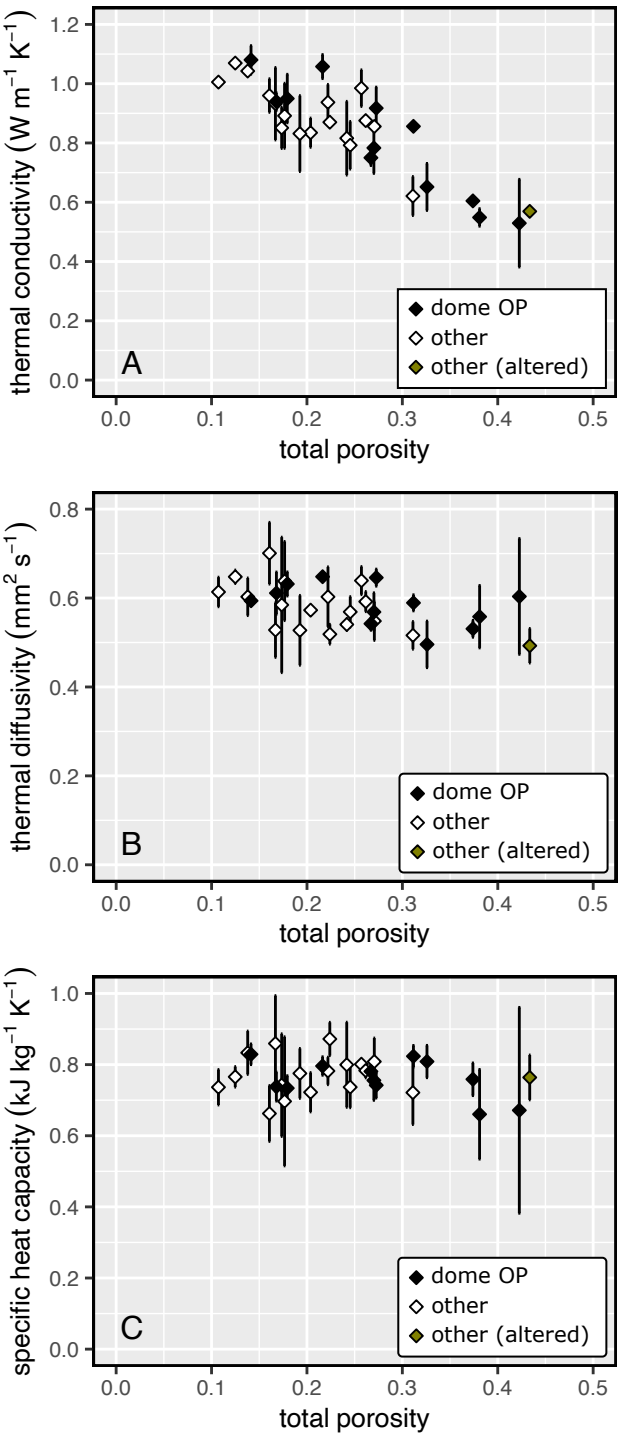

Figure 6: Thermal conductivity [A], thermal diffusivity [B], and specific heat capacity [C] as a function of total porosity for the suite of lavas from Havre volcano. Black diamonds - dome OP; white and yellow diamonds - other locations (see map in Figure 1 for sampling locations). Error bars show the standard deviation of the mean for the four measurements performed for each sample (see text for details).

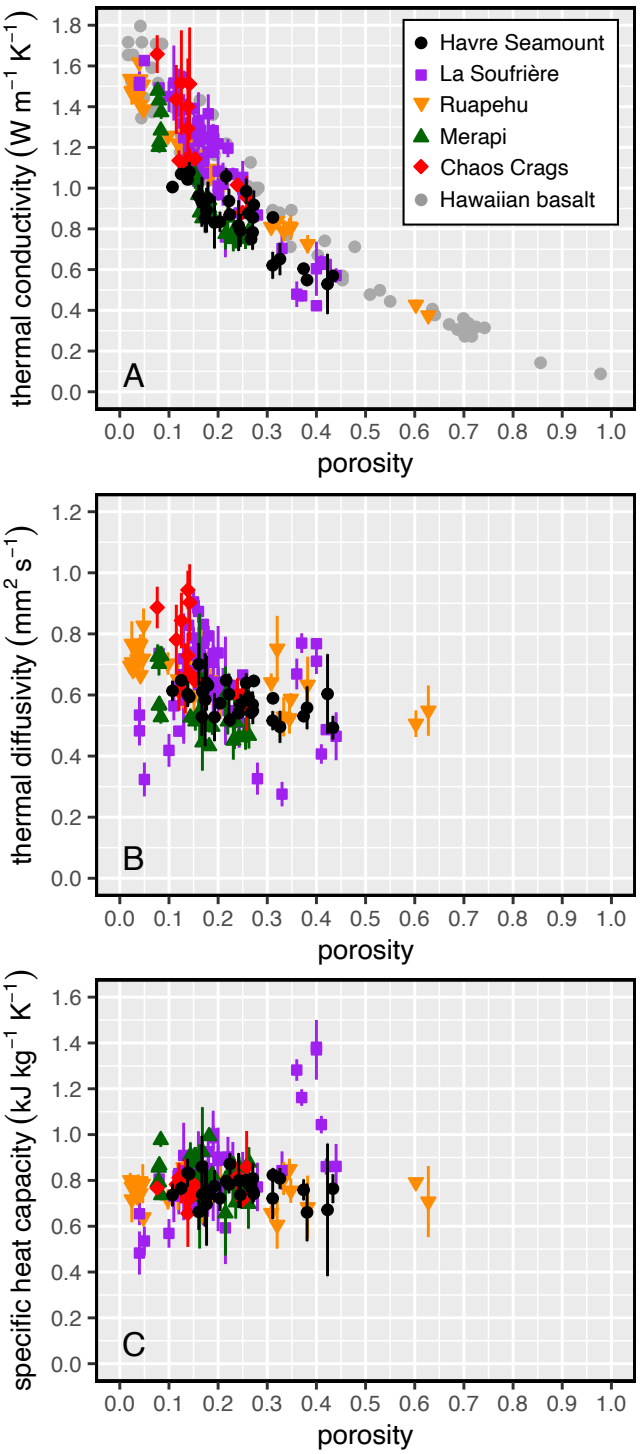

Figure 7: Thermal conductivity [A], thermal diffusivity [B], and specific heat capacity [C] as a function of total porosity for a suite of lavas from Havre volcano (black circles), alongside published data for andesites from La Soufrière de Guadeloupe (purple squares [Heap et al. 2022]) and Mt Ruapehu in New Zealand (orange downward-pointing triangles [Heap et al. 2020]), basaltic-andesites from Mt Merapi in Indonesia (green upward-pointing triangles [Heap et al. 2020]); dacites from Chaos Crags in USA (red diamonds [Heap et al. 2022]), and basalts from Hawai'i in the USA (grey circles [Robertson and Peck 1974]). Porosity values for the published data are connected porosities.

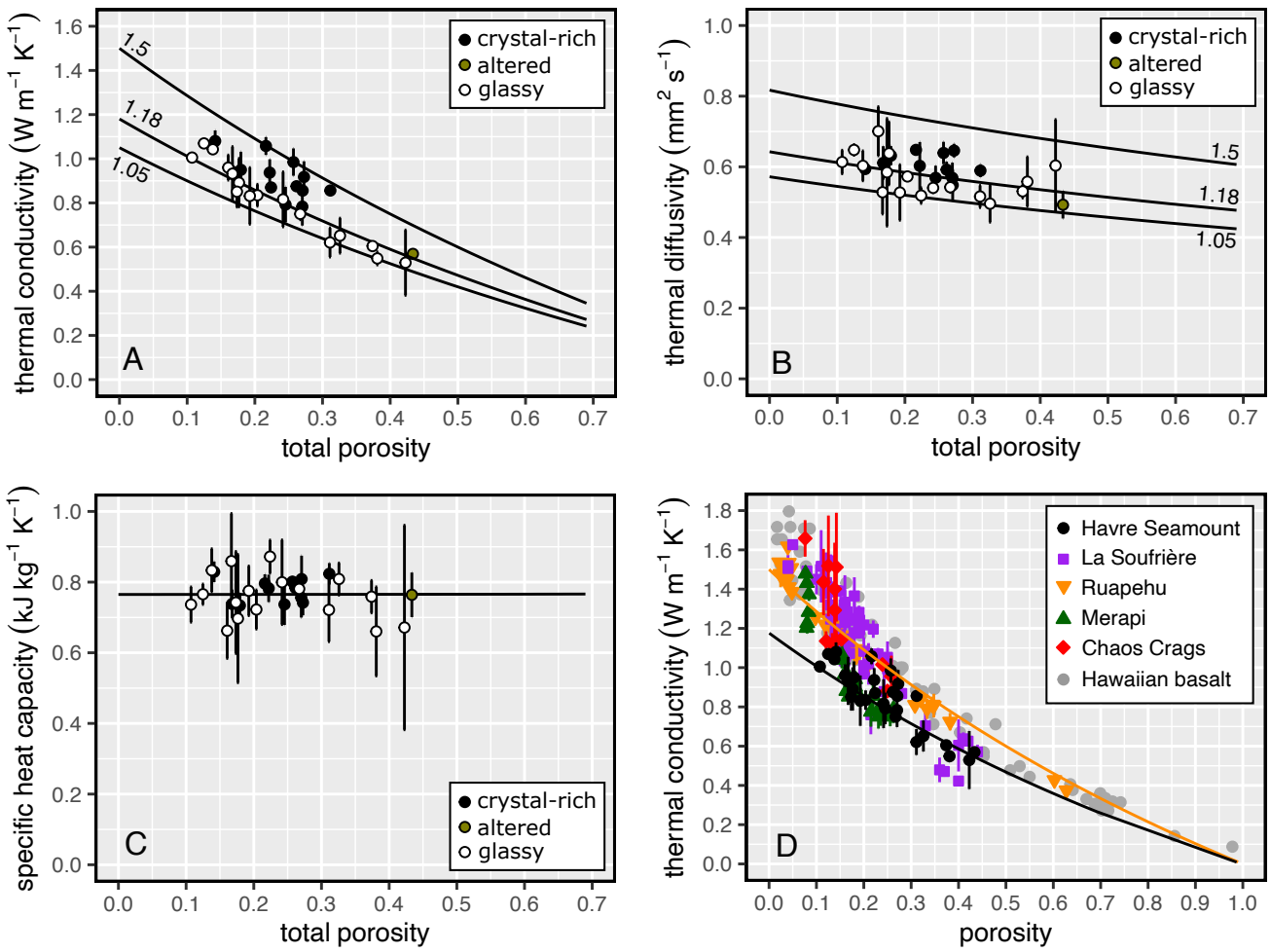

Figure 8: Thermal conductivity [A], thermal diffusivity [B], and specific heat capacity [C] as a function of total porosity for a suite of lavas from Havre volcano. The numbers next to the modelled curves in panels [A] and [B], provided using Equations 1–3, indicate the assumed rock groundmass conductivity, λ_0 (in W m^{-1} K^{-1}) (see text for details). [D] Thermal conductivity as a function of total porosity for a suite of lavas from Havre volcano (black circles), alongside published data for andesites from La Soufrière de Guadeloupe (purple squares [Heap et al. 2022]) and Mt Ruapehu in New Zealand (orange downward-pointing triangles [Heap et al. 2020]), basaltic-andesites from Mt Merapi in Indonesia (green upward-pointing triangles [Heap et al. 2020]); dacites from Chaos Crags in USA (red diamonds [Heap et al. 2022]), and basalts from Hawai'i in the USA (grey circles; Robertson and Peck 1974). Porosity values for the published data are connected porosities. Modelled best-fit curves are provided for the sample suite from Mt Ruapehu (orange curve; λ_0 = 1.5 W m^{-1} K^{-1} [Heap et al. 2020]) and for the lavas from Havre volcano (black curve; λ_0 = 1.18 W m^{-1} K^{-1}) (see text for details).

The effective thermal conductivity, $\lambda(\phi)$, can be determined using the Maxwell result for conduction in a medium containing inclusions (here the inclusions are pores):

$$\frac{\lambda(\phi)}{\lambda_0} = \frac{(1-\phi)(1-r)+r\beta\phi}{(1-\phi)(1-r)+\beta\phi}, \quad (1)$$

where ϕ is the porosity and $r = \lambda_f/\lambda_0$ (where λ_f and λ_0 and are the thermal conductivities of the pore-filling fluid and the rock groundmass, respectively [Zimmerman 1989]). We assume spherical pores, and so $\beta = 3(1-r)/(2+r)$ [Zimmerman 1989]. The effective thermal diffusivity $D(\phi)$ can then be determined using:

$$D(\phi) = \frac{\lambda(\phi)}{\rho_0 C_{p,0}(1-\phi)+\rho_f C_{p,f}\phi}, \quad (2)$$

where ρ_0 and ρ_f are the densities of the groundmass and pore fluid, respectively, and $C_{p,0}$ and $C_{p,f}$ are the specific heat capacity of the groundmass and pore fluid, respectively [Connor et al. 1997]. Based on Equation 2, the effective specific heat capacity $C_p(\phi)$ is given by the porosity-weighted average:

$$C_p(\phi) = \frac{\rho_0 C_{p,0}(1-\phi)+\rho_f C_{p,f}\phi}{\rho_b}. \quad (3)$$

We assume here a pore fluid thermal conductivity $\lambda_f = 0$ W m^{-1} K^{-1} (i.e. we assume that the condition of the porosity-filling air is negligible [Heap et al. 2020]). We take values of ρ_f and $C_{p,f}$ of 1.275 kg m^{-3} and 1.007 kJ kg^{-1} K^{-1} [Heap et al. 2020], respectively, and, guided by our experimental

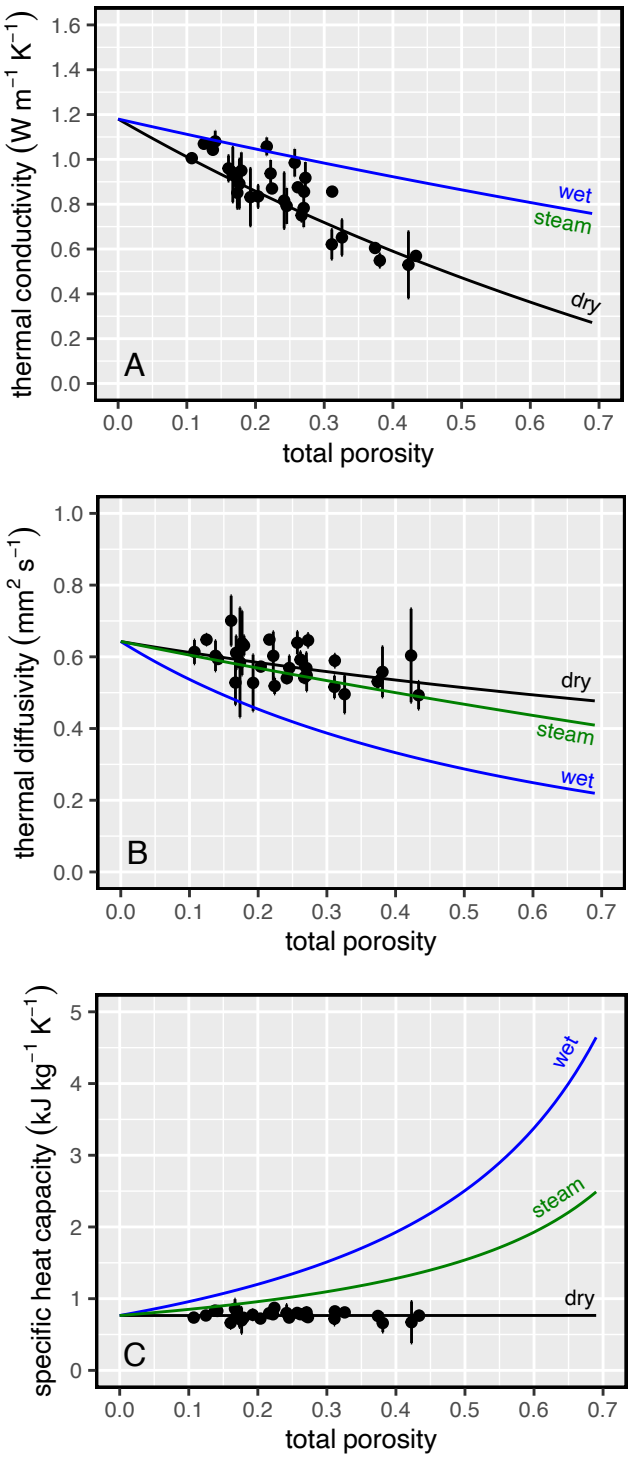

Figure 9: Thermal conductivity [A], thermal diffusivity [B], and specific heat capacity [C] as a function of total porosity for a suite of lavas from Havre volcano. The modelled curves provide predictions for the dry (black curves), water-saturated (blue curves), and steam-saturated (green) thermal properties (using Equations 1–3), assuming a rock groundmass conductivity, λ_0, of 1.18 W m^{-1} K^{-1} (see text for details).

data, we take values of ρ_0 and $C_{p,0}$ of 2400 kg m^{-3} and 0.765 kJ kg^{-1} K^{-1}, respectively. The key unknown then is λ_0.

We find that our thermal conductivity data for lavas from Havre volcano can be bracketed between modelled curves (using Equation 1) for which λ_0 equals 1.05 and 1.5 W m^{-1} K^{-1} (the black lines labelled "1.05" and "1.5", respectively, in Figure 8A). Using a least-squares regression analysis, we find a value of λ_0 of 1.18 ± 0.094 W m^{-1} K^{-1} best describes our complete dataset (the black line labelled "1.18" in Figure 8A). Using Equation 2, we can provide modelled curves for $D(\phi)$ using the same values of λ_0 (1.05, 1.18, and 1.5 W m^{-1} K^{-1}), as shown in Figure 8B. Finally, Figure 8C shows the modelled curve for the effective specific heat capacity (Equation 3). In general, we find that Equations 1–3, using the input values listed above and assuming λ_0 = 1.18 W m^{-1} K^{-1}, describe our complete dataset well (Figure 8).

Figure 8D shows the compiled thermal conductivity dataset (i.e. that presented in Figure 7A) with the modelled best-fit curves for the samples from Mt Ruapehu (orange curve; λ_0 = 1.5 W m^{-1} K^{-1} [Heap et al. 2020]) and for our new data for lavas from Havre volcano (black curve; λ_0 = 1.18 W m^{-1} K^{-1}). Heap et al. [2020] concluded that, because a suite of andesites with different microstructural parameters (e.g. different pore and crystal sizes and shapes) can be well described by Equations 1–3, porosity exerts the first-order control on the thermal properties and that all other microstructural parameters must only play a very minor role. Therefore, we conclude similarly for the lavas from Havre volcano as, despite their sample-to-sample microstructural differences (Figure 3), the data can be well described by Equations 1–3 (Figure 8). The fact that both volcanic rocks from subaerial volcanoes and those from Havre volcano can be well described by Equations 1–3 suggests that there are no fundamental differences between the thermal properties of volcanic rocks from submarine and subaerial volcanoes, and that the measured differences can be explained by differences in λ_0 (Figure 8D). Differences in λ_0 between the lavas from Havre volcano and the volcanic rocks from subaerial volcanoes must be the result of their different groundmass and mineral assemblages. The volcanic rocks from La Soufrière de Guadeloupe, Mt Ruapehu, Mt Merapi, and Chaos Crags are all porphyritic lavas characterised by either no or only small amounts of glass [Heap et al. 2020; 2022]. Some of the lavas from Havre volcano, by contrast, are very glassy (Figure 3). In Figure 8, we differentiate between the samples from Havre volcano that are glassy (white circles) and those that are crystal-rich (black circles); we note, however, that some of the crystal-rich samples are not completely devoid of glass. Importantly, the thermal conductivity of silica glass is much less than, for example, the thermal conductivity of plagioclase [Horai 1971; Clauser and Huenges 1995]. To support the hypothesis that a high glass content is the cause of the low best-fit λ_0 for the Havre volcano sample suite, and therefore the subtle difference between the volcanic rocks from subaerial volcanoes and those from Havre volcano, we additionally measured the thermal conductivity of porosity-free obsidian from Hrafntinnuhryggur (Krafla volcano, Iceland). We measured a value of 1.23 ± 0.009 W m^{-1} K^{-1} for the obsidian, very close to our best-fit λ_0 of 1.18 W m^{-1} K^{-1} for our suite of rocks from

Havre volcano (Figure 8). The thermal conductivity of obsidian from the Mono Craters (USA) was measured to be ~1.15 $W m^{-1} K^{-1}$ at room temperature [Romine et al. 2012], very close to our value of 1.23 $W m^{-1} K^{-1}$. Finally, we highlight that our most glassy samples have a lower thermal conductivity than the samples considered to be crystal-rich (Figure 8), corroborating the idea that glass content serves to lower the thermal conductivity.

Therefore, we conclude that there are essentially no differences between the thermal properties of volcanic rocks from subaerial volcanoes and those from Havre volcano, and that the lower values of thermal conductivity for a given porosity for the rocks from Havre volcano can simply be explained by their higher glass contents. This means that future studies that model heat transport in submarine volcanoes can use Equations 1–3 to provide thermal property values for modelling, provided that λ_0, the porosity, and the glass content (glassy or crystal-rich) of the rocks are known *a priori*.

5.2 Water- and steam-saturated thermal properties

We have provided thermal properties for oven-dry lava samples from Havre volcano (Figure 5). However, during eruption and emplacement, it is likely that the pore-filling phase changes from being a magmatic H_2O-dominated gas phase and, upon flow and cooling, that water (gas or liquid) fills the pores. At lower relative temperatures, it is very likely that these rocks would be water-saturated in-situ, and we know that saturation with water changes the thermal properties of rocks [Nagaraju and Roy 2014; Harlé et al. 2019], including volcanic rocks [Heap et al. 2020]. We therefore urge caution to those seeking thermal property values to model heat transport within submarine volcanoes just based on dry values obtained experimentally. However, we can estimate the water- and steam-saturated thermal properties of our sample suite using physically-grounded models (Equations 1–3), which allow us to extrapolate for the effect of liquid water or steam instead of gas. To do so, we assume values for liquid water of λ_f, ρ_f, and $C_{p,f}$ of 0.6 $W m^{-1} K^{-1}$, 1000 $kg m^{-3}$ and 4.182 $kJ kg^{-1} K^{-1}$, respectively, and values for steam of λ_f, ρ_f, and $C_{p,f}$ of 0.6 $W m^{-1} K^{-1}$, 997 $kg m^{-3}$ and 1.865 $kJ kg^{-1} K^{-1}$, respectively (values taken from the National Institute of Standards and Technology (NIST) Reference Fluid Thermodynamic and Transport Properties Database). The input parameters for liquid water, and Equations 1–3, have previously well described the thermal properties of completely water-saturated andesites from Mt Ruapehu [Heap et al. 2020], adding veracity to our approach. We highlight that, although some of the samples contain some minor isolated porosity (Figure 5), our approach assumes that all of the void space is saturated with liquid water or steam.

The modelled curves for the water- and steam-saturated thermal properties, using Equations 1–3, are shown in Figure 9 (blue and green curves, respectively). These model predictions show that water- and steam-saturation increases the thermal conductivity and the specific heat capacity, and decreases the thermal diffusivity. Saturation with water or steam increases the thermal conductivity by the same amount (Figure 9A), but the decrease in thermal diffusivity (Figure 9B) and the increase in specific heat capacity (Figure 9C) is greater for water- than for steam-saturation. We highlight that the difference between the dry and the water- or steam-saturated thermal properties increases as a function of porosity (Figure 9). For example, at a porosity of 0.1, the dry and wet thermal conductivity predicted by the model is 1.07 and 1.17 $W m^{-1} K^{-1}$, respectively, whereas the dry and wet thermal conductivity is 0.28 and 0.78 $W m^{-1} K^{-1}$, respectively, at a porosity of 0.7 (Figure 9A). Therefore, we recommend that future modelling endeavours that wish to use Equations 1–3 to provide thermal property values should first consider whether the rocks in question are dry, water-, or steam-saturated, and then use the corresponding values for the thermal properties of the fluid (air, water, or steam).

5.3 The effect of temperature

Before thermal conductivity values and constitutive models can be applied to magma cooling scenarios, the effect of temperature on the thermal properties must be established. To establish this, we compile data for thermal diffusivity from published sources for Little Glass Mountain obsidian at two porosities, $\phi = 0$ and $\phi \approx 0.75$ [Bagdassarov and Dingwell 1994]. We show constitutive models for these materials, which are: (1) for the Little Glass Mountain obsidian $D = A + BT + CT^2$, with $A = 9.14 \times 10^{-7}$, $B = 1.4 \times 10^{-9}$ and $C = 1.9 \times 10^{-12}$ for $\phi = 0$, and $A = 3.04 \times 10^{-7}$, $B = 2.9 \times 10^{-10}$, and 4×10^{-13} for $\phi \approx 0.75$; and (2) $\lambda = F \exp(GT)$ with $F = 1.88 \times 10^{-7}$ and $G = 1.58 \times 10^{-3}$ (and for this second model, T is in Kelvin and is from Wadsworth et al. [2017]). For this study, the limiting case of dense lava where $\phi = 0$ ($D \approx 6.8 \times 10^{-7}$ $m^2 s^{-1}$) matches very well with these prior constraints in other volcanic materials broadly in the range $20 \leq T \leq 700$ °C, where our constraint in within the reproducibility uncertainty of the previous data (Figure 10). We therefore conclude that the effect of temperature is minimal at these moderate to low temperatures, consistent with previous findings for Mt Shasta andesite [Hofmeister 2018]. Above 700 °C, the published $D(T)$ data diverge from our ambient temperature constraint by up to a factor of ~+1.4. However, the uncertainty in our D determinations combined with the uncertainties in Bagdassarov and Dingwell [1994] combine and lead us to conclude that the effect of temperature is minor, compared with the effect of porosity and saturation with water. Above 1000 °C, the effect of temperature appears to be pronounced, however it is unclear the extent to which this is due to the onset of a radiative component of heat transfer influencing the measurement (discussed in Bagdassarov and Dingwell [1994]), which can be corrected for [Whittington et al. 2009]. For this reason, in what follows, we will constrain our analysis to $T \leq 1000$ °C.

5.4 Conduction-limited lava crust development and the cooling of submarine lava domes

Conduction-limited lava crust development occurs perpendicular to the cooling surface over timescales τ_c proportional to:

$$\tau_c \propto \frac{L^2}{D}, \tag{4}$$

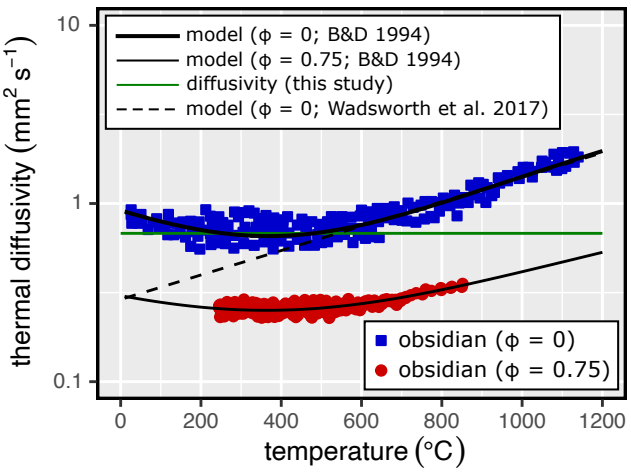

Figure 10: The temperature dependence of thermal diffusivity $D(T)$ shown using previously published data for obsidian at two porosities, $\phi = 0$ and $\phi \approx 0.75$. Best-fit empirical models for the effect of temperature are shown (see text). The horizontal line is our data at $\phi = 0$, showing that it is well within the uncertainty on previous data and approximately temperature independent up to around $T = 700$ °C.

where L is the length scale in question (here taken to be the lava crust thickness). This scaling $\tau_c(L)$ shows that the timescale relates to the diffusivity by $\tau_c \propto D^{-1}$. Therefore, in Figure 11A we show the predicted $\tau_c(L)$ for four cases using the scaling in Equation 4. First, the limiting case of dense lava where $\phi = 0$ ($D \approx 6.4 \times 10^{-7}$ m^2 s^{-1}). Second, for the case of a porous lava with $\phi = 0.5$ where the pore fluid is air ($D \approx 5.1 \times 10^{-7}$ m^2 s^{-1}). Third, for the case of a porous lava with $\phi = 0.5$ but where the pore fluid is liquid water ($D \approx 2.8 \times 10^{-7}$ m^2 s^{-1}). And, fourth, for the case of a porous lava with $\phi = 0.5$ but where the pore fluid is steam ($D \approx 4.7 \times 10^{-7}$ m^2 s^{-1}). The values of thermal diffusivity for these four cases were taken from the modelling presented in Figure 9B. This shows what can also be inferred from Figure 9B: that in this case, the effect of porosity is of second order, whereas the effect of void-filling liquid water is significant (Figure 11). However, if steam is the void-filling fluid, the cooling timescales are not dissimilar to those for the dry, porous lava (Figure 11). Our analysis also shows that a 0.1 m thick crust can conductively form in ~1–10 hours. To illustrate this further, we can solve for the temporal evolution of temperature $T(t)$ at the 0.1 m depth in the lava from the cooling surface using an analytical solution to Fick's second law:

$$T(t) = T_i + (T_e - T_i)\,\mathrm{erfc}(\zeta), \qquad (5)$$

where T_i is the initial temperature, T_e is the equilibrium temperature, and $\zeta^2 = L^2/(4Dt)$ with t the time since the onset of cooling. The assumptions that underpin Equation 5 are that the boundary at the lava cooling surface are conductively losing heat into the fluid, and that the lava itself is a semi-infinite domain. For illustrative purposes, if we take $T_i = 1000$ °C, $T_e = 20$ °C, and $L = 0.1$ m, then we find that the time required for the temperature to reach the glass transition $T_g \approx 780$ °C is ~1.4 hours, ~1.7 hours, ~2 hours, and ~5 hours, for the dense, porous-water, porous-steam, and porous-air cases discussed above, respectively (Figure 11B). This is an example of how the thermal properties constrained herein can be used to solve relatively simple conduction problems. In concert with full conduction-convection solutions to heat transfer problems, these constraints can represent what is needed to predict the evolution of temperature distribution in submarine lavas.

To confirm that submarine lavas are conductively limited in their cooling behaviour, we define the Biot number B i= hL/λ where h is the heat transfer coefficient for water. In principle, if Bi $\ll 1$, then the thermal conductivity is sufficiently large that conduction within the material lava is more efficient than heat loss into the water through the cooling surface. By contrast, if Bi $\gg 1$, then conduction is relatively inefficient and the system will be conduction-limited [Wadsworth et al. 2017; Moitra et al. 2020]. If we take $h \approx 10^3$ W m^{-1} K^{-1} [Moitra et al. 2020] and a characteristic value $\lambda \approx 1$ W m^{-1} K^{-1}, we can rearrange Bi for the critical length scale L_c for a transition between Bi < 1 (surface heat transfer–limited) and Bi >1 (conduction-limited), as $L_c = \lambda/h = 0.001$ m. According to this simple analysis, anything larger than this length scale L_c will typically be conduction limited in the submarine realm. Therefore, as a first step in understanding the cooling of lava-sized bodies and their developing crusts, solving conduction-limited cooling is necessary, and the relatively simplistic scaling for τ_c is approximately valid (Figure 11).

Of course, this analysis (e.g. Equation 5) is simplistic and more sophisticated approaches are needed and indeed exist [e.g. Griffiths 2000]. In real submarine realms, the convection boundary condition may well be more involved than the Biot number analysis given above, and phase changes, boundary layers, and thermal instabilities may all be important effects in submarine lava cooling [Griffiths 2000; Moitra et al. 2020; Moitra and Sonder 2022]. However, we propose that there is value in exploring the conduction-limited effects of different thermal properties constrained here simply to illustrate the important effects of these thermal properties. Griffiths [2000] provide a framework for understanding lava advance in a range of conditions, but do not have good constraints of the thermal properties for any specific case or scenario. Here, the properties will be necessary to place sophisticated thermal models on firm footing in the future.

The conduction limited cooling history of a lava crust can inform the understanding of heat flux to the ambient environment, and coupled with other parameters such as magma viscosity, effusion rate, and slope can inform lava flow morphology and mobility. Fauria and Manga [2018] demonstrate that hot porous pumice clasts cool by the production of steam in the void space, heat loss to the surroundings causing condensation of internal vapour, and clast saturation. Conceptually, the same process is likely responsible for the cooling of larger scale lavas and domes, forming a steam and liquid water "blanket" in the outer porous carapace of the lava or dome. This blanket effectively insulates the interior of a degassing lava body from the ambient water environment, trapping hot magmatic volatiles internally within the lava or dome, and facilitating longer timescales of cooling, and subsequent

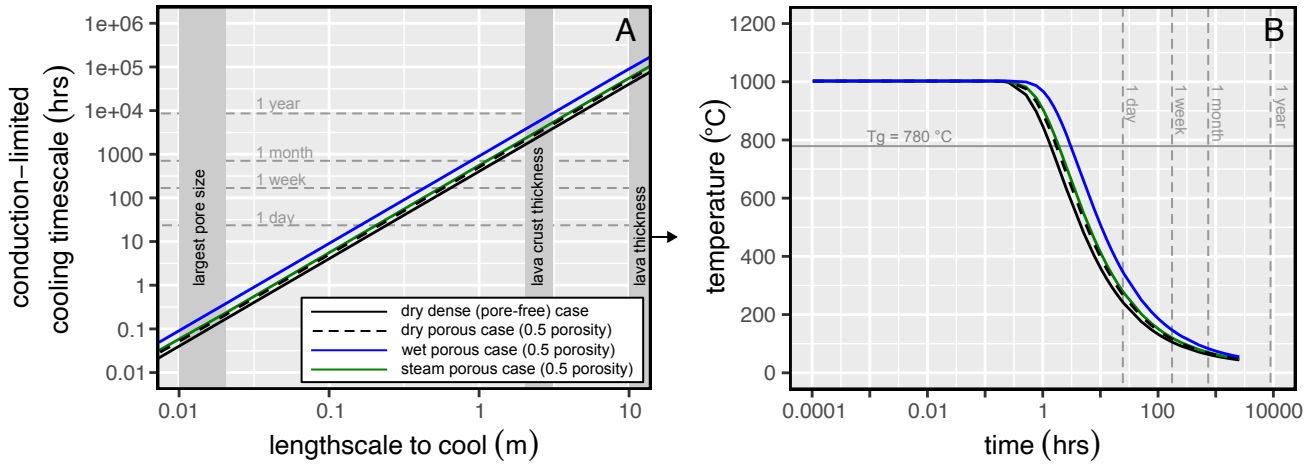

Figure 11: [A] The conduction scaling $\tau_c = L^2/D$ for four cases: (1) the dry dense lava case where $D \approx 6.4 \times 10^{-7}$ m^2 s^{-1} (solid black curve); (2) the dry porous lava case where $D \approx 5.1 \times 10^{-7}$ m^2 s^{-1} (dashed black curve); (3) the porous lava case with water as the pore-filling fluid where $D \approx 2.8 \times 10^{-7}$ m^2 s^{-1} (solid blue curve); and (4) the porous lava case with steam as the pore-filling fluid where $D \approx 4.7 \times 10^{-7}$ m^2 s^{-1} (solid green curve). [B] The analytical solution to Fick's second law for $T(t)$ for a fixed L = 0.1 m (see text). Indicated on panel [A] are the length scales for the largest pore size (10–20 mm), the average lava crust thickness (2–3 m), and the total lava thickness (from 10 m up to a couple of hundred metres).

vesiculation, crystallisation, and cristobalite precipitation. The thermal gradients of lavas and domes are therefore complex spatially and with time, which makes modelling of lava cooling and saturation in water a complex problem.

6 Conclusions

We provide here laboratory-measured thermal property values for a suite of lavas from a submarine volcano, Havre volcano in the Kermadec Ridge (Pacific Ocean). We find that their thermal conductivity decreases (from ~1.1 to ~0.5 W m^{-1} K^{-1}) as total porosity is increased from ~0.1 to ~0.45. However, we also find that their thermal diffusivity (0.5–0.7 mm^2 s^{-1}) and specific heat capacity (0.65–0.9 J kg^{-1} K^{-1}) do not change systematically as a function of porosity. By comparing our new data for a submarine volcano with those previously published for subaerial volcanoes we find that, although both data types can be well described by physically-grounded effective medium approaches, the thermal conductivity of the lavas from Havre volcano are lower than those from subaerial volcanoes for a given porosity. The reason for this difference is that the lavas from Havre volcano are glassier, an amorphous solid with a low thermal conductivity, than the rocks measured from subaerial volcanoes. We do not suggest, however, that there are differences, in terms of their thermal properties, between rocks from submarine and subaerial volcanoes, and we expect that glassier samples from subaerial volcanoes would have thermal properties similar to the submarine lavas measured herein. Using the effective medium models, we can determine the thermal properties of the measured sample suite under water-saturated conditions, a perhaps more realistic scenario for lavas comprising a submarine volcano. We find that saturation with water increases their thermal conductivity and specific heat capacity and decreases their thermal diffusivity. Using the data and models provided herein, the thermal properties of any lava can be estimated as long as the thermal conductivity at zero porosity (λ_0)—which requires an understanding as to whether the sample is glassy or crystal-rich—the porosity, and the nature of the void-filling fluid (air, steam, or water) are known. This approach can, therefore, be used in multiphase models for submarine eruption dynamics, hydrothermal system hydrology, cooling timescales—as we discuss above—and the heat flux from the global mid-ocean ridge system to the ocean. The use of more accurate values for the thermal properties of submarine lavas in such models will lead to more reliable model outputs.

Author Contributions

RC and MH led the writing of the article. RJC and SM collected the samples. RJC collected the SEM images and described their textural properties. MH collected the experimental data. FB performed the cooling modelling. All authors contributed to discussions and concepts described in the article, providing input and revisions to earlier versions of the manuscript.

Acknowledgements

We thank the captain, operations teams, marine technicians, and crew of the R/V Roger Revelle and the operations team of the ROV Jason and the AUV Sentry for their expert help at sea collecting these samples. We thank S. Feig, K. Goemann, and staff of the Central Science Laboratory at the University of Tasmania. M. Heap was supported by ANR grant MYGALE ("Modelling the phYsical and chemical Gradients of hydrothermal ALteration for warning systems of flank collapse at Explosive volcanoes"; ANR-21-CE49-0010) and a European Research Council Synergy Grant (ERC-ROTTnROCK-101118491). M. Heap also acknowledges support from the Institut Universitaire de France (IUF). We thank Bertrand

Renaudie and Sharon Allen for sample preparation. We thank Yassine Derhem and Samya Charbonnel. This research was funded by Australian Research Council Linkage Grant LP190100478. The comments of two anonymous reviewers helped improve this manuscript.

Data Availability

The data collected for this study are available in the Microsoft Excel spreadsheet that accompanies this contribution. An additional supplementary file contains a photograph of each block in-situ (taken by the ROV during sample collection), a photograph of each block, and additional backscattered scanning electron microscope images for each block.

Copyright Notice

References

Annen, C. (2017). "Factors Affecting the Thickness of Thermal Aureoles". *Frontiers in Earth Science* 5. DOI: 10.3389/feart.2017.00082.

Annen, C., M. Pichavant, O. Bachmann, and A. Burgisser (2008). "Conditions for the growth of a long-lived shallow crustal magma chamber below Mount Pelee volcano (Martinique, Lesser Antilles Arc)". *Journal of Geophysical Research: Solid Earth* 113(B7). DOI: 10.1029/2007jb005049.

Bagdassarov, N. and D. Dingwell (1994). "Thermal properties of vesicular rhyolite". *Journal of Volcanology and Geothermal Research* 60(2), pages 179–191. DOI: 10.1016/0377-0273(94)90067-1.

Balkan, E., K. Erkan, and M. Şalk (2017). "Thermal conductivity of major rock types in western and central Anatolia regions, Turkey". *Journal of Geophysics and Engineering* 14(4), pages 909–919. DOI: 10.1088/1742-2140/aa5831.

Bruce, P. M. and H. E. Huppert (1989). "Thermal control of basaltic fissure eruptions". *Nature* 342(6250), pages 665–667. DOI: 10.1038/342665a0.

Burchardt, S., M. Bazargan, E. Bessi Gestsson, C. Hieronymus, E. Ronchin, H. Tuffen, M. J. Heap, J. Davidson, B. Kennedy, A. Hobé, and E. Saubin (2022). "Geothermal potential of small sub-volcanic intrusions in a typical Icelandic caldera setting". *Volcanica* 5(2), pages 477–507. DOI: 10.30909/vol.05.02.477507.

Canet, C., F. Trillaud, R. M. Prol-Ledesma, G. González-Hernández, B. Peláez, B. Hernández-Cruz, and M. M. Sánchez-Córdova (2015). "Thermal history of the Acoculco geothermal system, eastern Mexico: Insights from numerical modeling and radiocarbon dating". *Journal of Volcanology and Geothermal Research* 305, pages 56–62. DOI: 10.1016/j.jvolgeores.2015.09.019.

Carey, R. J., S. A. Soule, M. Manga, J. D. L. White, J. McPhie, R. Wysoczanski, M. Jutzeler, K. Tani, D. Yoerger, D. Fornari, F. Caratori-Tontini, B. Houghton, S. Mitchell, F. Ikegami, C. Conway, A. Murch, K. Fauria, M. P. Jones, R. Cahalan, and W. McKenzie (2018). "The largest deep-ocean silicic volcanic eruption of the past century". *Science Advances* 4(1). DOI: 10.1126/sciadv.1701121.

Carey, R. J., R. Wysoczanski, R. Wunderman, and M. Jutzeler (2014). "Discovery of the Largest Historic Silicic Submarine Eruption". *Eos, Transactions American Geophysical Union* 95(19), pages 157–159. DOI: 10.1002/2014eo190001.

Carlino, S., A. Troiano, M. G. Di Giuseppe, A. Tramelli, C. Troise, R. Somma, and G. De Natale (2016). "Exploitation of geothermal energy in active volcanic areas: A numerical modelling applied to high temperature Mofete geothermal field, at Campi Flegrei caldera (Southern Italy)". *Renewable Energy* 87, pages 54–66. DOI: 10.1016/j.renene.2015.10.007.

Carrigan, C. R. (1984). "Time and temperature dependent convection models of cooling reservoirs: Application to volcanic sills". *Geophysical Research Letters* 11(8), pages 693–696. DOI: 10.1029/gl011i008p00693.

Carrigan, C. R., G. Schubert, and J. C. Eichelberger (1992). "Thermal and dynamical regimes of single- and two-phase magmatic flow in dikes". *Journal of Geophysical Research: Solid Earth* 97(B12), pages 17377–17392. DOI: 10.1029/92jb01244.

Clauser, C. and E. Huenges (1995). "Thermal Conductivity of Rocks and Minerals". *Rock Physics & Phase Relations*. Edited by T. J. Ahrens. American Geophysical Union, pages 105–126. DOI: 10.1029/rf003p0105.

Connor, C. B., P. C. Lichtner, F. M. Conway, B. E. Hill, A. A. Ovsyannikov, I. Federchenko, Y. Doubik, V. N. Shapar, and Y. A. Taran (1997). "Cooling of an igneous dike 20 yr after intrusion". *Geology* 25(8), page 711. DOI: 10.1130/0091-7613(1997)025<0711:coaidy>2.3.co;2.

Fauria, K. E. and M. Manga (2018). "Pyroclast cooling and saturation in water". *Journal of Volcanology and Geothermal Research* 362, pages 17–31. DOI: 10.1016/j.jvolgeores.2018.07.002.

Fialko, Y. A. and A. M. Rubin (1999). "Thermal and mechanical aspects of magma emplacement in giant dike swarms". *Journal of Geophysical Research: Solid Earth* 104(B10), pages 23033–23049. DOI: 10.1029/1999jb900213.

Fujii, N. and M. Osako (1973). "Thermal diffusivity of lunar rocks under atmospheric and vacuum conditions". *Earth and Planetary Science Letters* 18(1), pages 65–71. DOI: 10.1016/0012-821x(73)90035-6.

Global Volcanism Program (GVP) (2012). "Report on Havre Seamount (New Zealand)". *Bulletin of the Global Volcanism Network*. Edited by R. Wunderman. Volume 37. 9. Smithsonian Institution. DOI: 10.5479/si.gvp.bgvn201209-242005.

González, J., C. E. Zambra, L. González, B. Clausen, and D. A. Vasco (2022). "Simulation of cooling in a magma chamber: Implications for geothermal fields of southern Peru". *Geothermics* 105, page 102515. DOI: 10.1016/j.geothermics.2022.102515.

Griffiths, R. W. (2000). "The Dynamics of Lava Flows". *Annual Review of Fluid Mechanics* 32(1), pages 477–518. DOI: 10.1146/annurev.fluid.32.1.477.

Griffiths, R. W. and J. H. Fink (1992). "The morphology of lava flows in planetary environments: Predictions from analog experiments". *Journal of Geophysical Research: Solid Earth* 97(B13), pages 19739–19748. DOI: 10.1029/92jb01953.

Gunnarsson, G. and E. S. P. Aradóttir (2015). "The Deep Roots of Geothermal Systems in Volcanic Areas: Boundary Conditions and Heat Sources in Reservoir Modeling". *Transport in Porous Media* 108(1), pages 43–59. DOI: 10.1007/s11242-014-0328-1.

Gustafsson, S. E. (1991). "Transient plane source techniques for thermal conductivity and thermal diffusivity measurements of solid materials". *Review of Scientific Instruments* 62(3), pages 797–804. DOI: 10.1063/1.1142087.

Hammerschmidt, U. and W. Sabuga (2000). *International Journal of Thermophysics* 21(1), pages 217–248. DOI: 10.1023/a:1006621324390.

Harlé, P., A. R. L. Kushnir, C. Aichholzer, M. J. Heap, R. Hehn, V. Maurer, P. Baud, A. Richard, A. Genter, and P. Duringer (2019). "Heat flow density estimates in the Upper Rhine Graben using laboratory measurements of thermal conductivity on sedimentary rocks". *Geothermal Energy* 7(1). DOI: 10.1186/s40517-019-0154-3.

Heap, M. J., D. E. Jessop, F. B. Wadsworth, M. Rosas-Carbajal, J.-C. Komorowski, H. A. Gilg, N. Aron, M. Buscetti, L. Gential, M. Goupil, M. Masson, L. Hervieu, A. R. Kushnir, P. Baud, L. Carbillet, A. G. Ryan, and R. Moretti (2022). "The thermal properties of hydrothermally altered andesites from La Soufrière de Guadeloupe (Eastern Caribbean)". *Journal of Volcanology and Geothermal Research* 421, page 107444. DOI: 10.1016/j.jvolgeores.2021.107444.

Heap, M. J., A. R. Kushnir, J. Vasseur, F. B. Wadsworth, P. Harlé, P. Baud, B. M. Kennedy, V. R. Troll, and F. M. Deegan (2020). "The thermal properties of porous andesite". *Journal of Volcanology and Geothermal Research* 398, page 106901. DOI: 10.1016/j.jvolgeores.2020.106901.

Heap, M. J., F. B. Wadsworth, and D. E. Jessop (2023). "The thermal conductivity of unlithified granular volcanic materials: The influence of hydrothermal alteration and degree of water saturation". *Journal of Volcanology and Geothermal Research* 435, page 107775. DOI: 10.1016/j.jvolgeores.2023.107775.

Hofmeister, A. M. (2018). *Measurements, mechanisms, and models of heat transport*. 1st Edition. Elsevier. 440 pages. ISBN: 9780128099810.

Hofmeister, A. M., A. Sehlke, G. Avard, A. J. Bollasina, G. Robert, and A. G. Whittington (2016). "Transport properties of glassy and molten lavas as a function of temperature and composition". *Journal of Volcanology and Geothermal Research* 327, pages 330–348. DOI: 10.1016/j.jvolgeores.2016.08.015.

Horai, K.-I. (1971). "Thermal conductivity of rock-forming minerals". *Journal of Geophysical Research* 76(5), pages 1278–1308. DOI: 10.1029/jb076i005p01278.

Horai, K.-I., G. Simmons, H. Kanamori, and D. Wones (1970). "Thermal Diffusivity and Conductivity of Lunar Material". *Science* 167(3918), pages 730–731. DOI: 10.1126/science.167.3918.730.

Huppert, H. E. and R. S. J. Sparks (1981). "The fluid dynamics of a basaltic magma chamber replenished by influx of hot, dense ultrabasic magma". *Contributions to Mineralogy and Petrology* 75(3), pages 279–289. DOI: 10.1007/bf01166768.

Ikegami, F., J. McPhie, R. Carey, R. Mundana, A. Soule, and M. Jutzeler (2018). "The Eruption of Submarine Rhyolite Lavas and Domes in the Deep Ocean – Havre 2012, Kermadec Arc". *Frontiers in Earth Science* 6. DOI: 10.3389/feart.2018.00147.

Irvine, T. N. (1970). "Heat transfer during solidification of layered intrusions. I. Sheets and sills". *Canadian Journal of Earth Sciences* 7(4), pages 1031–1061. DOI: 10.1139/e70-098.

Jutzeler, M., R. Marsh, R. J. Carey, J. D. L. White, P. J. Talling, and L. Karlstrom (2014). "On the fate of pumice rafts formed during the 2012 Havre submarine eruption". *Nature Communications* 5(1). DOI: 10.1038/ncomms4660.

Lenhardt, N. and A. E. Götz (2015). "Geothermal reservoir potential of volcaniclastic settings: The Valley of Mexico, Central Mexico". *Renewable Energy* 77, pages 423–429. DOI: 10.1016/j.renene.2014.12.034.

Loncar, M. and H. E. Huppert (2022). "Dyke cooling upon intrusion: Subsequent shape change, cooling regimes and the effect of further magma input". *Earth and Planetary Science Letters* 593, page 117687. DOI: 10.1016/j.epsl.2022.117687.

Manga, M., K. E. Fauria, C. Lin, S. J. Mitchell, M. P. Jones, C. E. Conway, W. Degruyter, B. Hosseini, R. Carey, R. Cahalan, B. F. Houghton, J. D. White, M. Jutzeler, S. A. Soule, and K. Tani (2018a). "The pumice raft-forming 2012 Havre submarine eruption was effusive". *Earth and Planetary Science Letters* 489, pages 49–58. DOI: 10.1016/j.epsl.2018.02.025.

Manga, M., S. J. Mitchell, W. Degruyter, and R. J. Carey (2018b). "Transition of eruptive style: Pumice raft to dome-forming eruption at the Havre submarine volcano, southwest Pacific Ocean". *Geology* 46(12), pages 1075–1078. DOI: 10.1130/g45436.1.

Mielke, P., K. Bär, and I. Sass (2017). "Determining the relationship of thermal conductivity and compressional wave velocity of common rock types as a basis for reservoir characterization". *Journal of Applied Geophysics* 140, pages 135–144. DOI: 10.1016/j.jappgeo.2017.04.002.

Mielke, P., M. Nehler, G. Bignall, and I. Sass (2015). "Thermophysical rock properties and the impact of advancing hydrothermal alteration — A case study from the Tauhara geothermal field, New Zealand". *Journal of Volcanology and Geothermal Research* 301, pages 14–28. DOI: 10.1016/j.jvolgeores.2015.04.007.

Mielke, P., S. Weinert, G. Bignall, and I. Sass (2016). "Thermophysical rock properties of greywacke basement rock and intrusive lavas from the Taupo Volcanic Zone, New Zealand". *Journal of Volcanology and Geothermal Re-*

search 324, pages 179–189. DOI: 10.1016/j.jvolgeores.2016.06.002.

Moitra, P. and I. Sonder (2022). "Vapor Bubbles and Velocity Control on the Cooling Rates of Lava and Pyroclasts During Submarine Eruptions". *Journal of Geophysical Research: Solid Earth* 127(8). DOI: 10.1029/2022jb024665.

Moitra, P., I. Sonder, and G. A. Valentine (2020). "The role of external water on rapid cooling and fragmentation of magma". *Earth and Planetary Science Letters* 537, page 116194. DOI: 10.1016/j.epsl.2020.116194.

Nabelek, P. I., A. M. Hofmeister, and A. G. Whittington (2012). "The influence of temperature-dependent thermal diffusivity on the conductive cooling rates of plutons and temperature-time paths in contact aureoles". *Earth and Planetary Science Letters* 317–318, pages 157–164. DOI: 10.1016/j.epsl.2011.11.009.

Nagaraju, P. and S. Roy (2014). "Effect of water saturation on rock thermal conductivity measurements". *Tectonophysics* 626, pages 137–143. DOI: 10.1016/j.tecto.2014.04.007.

Norton, D. and J. E. Knight (1977). "Transport phenomena in hydrothermal systems; cooling plutons". *American Journal of Science* 277(8), pages 937–981. DOI: 10.2475/ajs.277.8.937.

Robertson, E. C. and D. L. Peck (1974). "Thermal conductivity of vesicular basalt from Hawaii". *Journal of Geophysical Research* 79(32), pages 4875–4888. DOI: 10.1029/jb079i032p04875.

Romine, W. L., A. G. Whittington, P. I. Nabelek, and A. M. Hofmeister (2012). "Thermal diffusivity of rhyolitic glasses and melts: effects of temperature, crystals and dissolved water". *Bulletin of Volcanology* 74(10), pages 2273–2287. DOI: 10.1007/s00445-012-0661-6.

Spain, E., R. J. Carey, J. M. Whittaker, V. L. Lucieer, J. M. Fox, S. J. Watson, and F. C. Tontini (2025). "Geomorphic time series reveals the constructive and destructive history of Havre caldera volcano, Kermadec arc". *Frontiers in Earth Science* 12. DOI: 10.3389/feart.2024.1463257.

Tsang, S. W. R., J. M. Lindsay, G. Coco, R. Wysocki, G. A. Lerner, E. Rader, G. M. Turner, and B. Kennedy (2019). "The heating of substrates beneath basaltic lava flows". *Bulletin of Volcanology* 81(11). DOI: 10.1007/s00445-019-1320-y.

Vélez, M. I., D. Blessent, S. Córdoba, J. López-Sánchez, J. Raymond, and E. Parra-Palacio (2018). "Geothermal potential assessment of the Nevado del Ruiz volcano based on rock thermal conductivity measurements and numerical modeling of heat transfer". *Journal of South American Earth Sciences* 81, pages 153–164. DOI: 10.1016/j.jsames.2017.11.011.

Wadsworth, F. B., J. Vasseur, E. W. Llewellin, K. Genareau, C. Cimarelli, and D. B. Dingwell (2017). "Size limits for rounding of volcanic ash particles heated by lightning". *Journal of Geophysical Research: Solid Earth* 122(3), pages 1977–1989. DOI: 10.1002/2016jb013864.

Weydt, L. M., F. Lucci, A. Lacinska, D. Scheuvens, G. Carrasco-Núñez, G. Giordano, C. A. Rochelle, S. Schmidt, K. Bär, and I. Sass (2022). "The impact of hydrothermal alteration on the physiochemical characteristics of reservoir rocks: the case of the Los Humeros geothermal field (Mexico)". *Geothermal Energy* 10(1). DOI: 10.1186/s40517-022-00231-5.

Weydt, L. M., Á. A. Ramírez-Guzmán, A. Pola, B. Lepillier, J. Kummerow, G. Mandrone, C. Comina, P. Deb, G. Norini, E. Gonzalez-Partida, D. R. Avellán, J. L. Macías, K. Bär, and I. Sass (2021). "Petrophysical and mechanical rock property database of the Los Humeros and Acoculco geothermal fields (Mexico)". *Earth System Science Data* 13(2), pages 571–598. DOI: 10.5194/essd-13-571-2021.

White, J. D., J. McPhie, and S. A. Soule (2015). "Submarine Lavas and Hyaloclastite". *The Encyclopedia of Volcanoes*. Elsevier, pages 363–375. ISBN: 9780123859389. DOI: 10.1016/b978-0-12-385938-9.00019-5.

Whittington, A. G., A. M. Hofmeister, and P. I. Nabelek (2009). "Temperature-dependent thermal diffusivity of the Earth's crust and implications for magmatism". *Nature* 458(7236), pages 319–321. DOI: 10.1038/nature07818.

Wooster, M. J., R. Wright, S. Blake, and D. A. Rothery (1997). "Cooling mechanisms and an approximate thermal budget for the 1991–1993 Mount Etna lava flow". *Geophysical Research Letters* 24(24), pages 3277–3280. DOI: 10.1029/97gl03166.

Wright, I., T. Worthington, and J. Gamble (2006). "New multibeam mapping and geochemistry of the 30°–35° S sector, and overview, of southern Kermadec arc volcanism". *Journal of Volcanology and Geothermal Research* 149(3–4), pages 263–296. DOI: 10.1016/j.jvolgeores.2005.03.021.

Yokose, H., P. W. Lipman, and T. Kanamatsu (2005). "Physical and chemical properties of submarine basaltic rocks from the submarine flanks of the Hawaiian Islands". *Marine Geology* 219(2–3), pages 173–193. DOI: 10.1016/j.margeo.2005.05.005.

Zimmerman, R. W. (1989). "Thermal conductivity of fluid-saturated rocks". *Journal of Petroleum Science and Engineering* 3(3), pages 219–227. DOI: 10.1016/0920-4105(89)90019-3.